AD-A174 462 THE EFFECT OF SURFACE ORIENTATION ON SILICON OXIDATION KINETICS(U) NORTH CAROLINA UNIV AT CHAPEL HILL DEPT OF CHEMISTRY E A LEWIS ET AL 13 NOV 86 TR-12 1/1

UNCLASSIFIED N00014-86-K-0305 F/G 7/4 NL

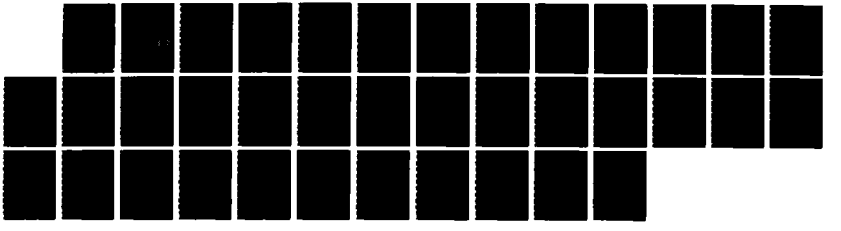

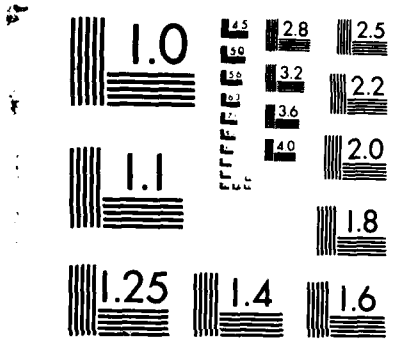

MICROCOPY RESOLUTION TEST CHART
NATIONAL BUREAU OF STANDARDS-1963-A

12

OFFICE OF NAVAL RESEARCH

Contract No. N00014-86-K-0305

TECHNICAL REPORT NO. 12

The Effect of Surface Orientation on Silicon Oxidation Kinetics

by

E A. Lewis and E.A. Irene
Department of Chemistry
The University of North Carolina
Chapel Hill, North Carolina 27514

in

The Journal of Electrochemical Society (submitted)

SECURITY CLASSIFICATION OF THIS PAGE

REPORT DOCUMENTATION PAGE

1a REPORT SECURITY CLASSIFICATION Unclassified	1b RESTRICTIVE MARKINGS
2a SECURITY CLASSIFICATION AUTHORITY	3 DISTRIBUTION/AVAILABILITY OF REPORT Approved for public release; distribution unlimited
2b DECLASSIFICATION/DOWNGRADING SCHEDULE	
4 PERFORMING ORGANIZATION REPORT NUMBER(S) Technical Report #12	5. MONITORING ORGANIZATION REPORT NUMBER(S)
6a NAME OF PERFORMING ORGANIZATION UNC Chemistry Dept. 6b OFFICE SYMBOL (If applicable)	7a. NAME OF MONITORING ORGANIZATION Office of Naval Research (Code 413)
6c ADDRESS (City, State, and ZIP Code) 11-3 Venable Hall 045A Chapel Hill, NC 27514	7b ADDRESS (City, State, and ZIP Code) Chemistry Program 800 N. Quincy Street Arlington, Virginia 22217
8a NAME OF FUNDING/SPONSORING ORGANIZATION Office of Naval Research 8b OFFICE SYMBOL (If applicable)	9 PROCUREMENT INSTRUMENT IDENTIFICATION NUMBER Contract #N00014-86-K-0305
8c ADDRESS (City, State, and ZIP Code) Chemistry Program 800 N. Quincy, Arlington, VA 22217	10 SOURCE OF FUNDING NUMBERS PROGRAM ELEMENT NO / PROJECT NO / TASK NO. / WORK UNIT ACCESSION NO.

11 TITLE (Include Security Classification)

THE EFFECT OF SURFACE ORIENTATION ON SILICON OXIDATION KINETICS

12 PERSONAL AUTHOR(S)

E.A. Lewis and E.A. Irene

13a TYPE OF REPORT	13b TIME COVERED	14 DATE OF REPORT (Year, Month, Day)	15 PAGE COUNT
Interim Technical	FROM _____ TO _____	11/13/86	34

16 SUPPLEMENTARY NOTATION

Prepared for publication in The Journal of Science and Technology

17 COSATI CODES			18 SUBJECT TERMS (Continue on reverse if necessary and identify by block number)
FIELD	GROUP	SUB-GROUP	

19 ABSTRACT (Continue on reverse if necessary and identify by block number)

It is well established that the rate of thermal oxidation of silicon depends on the surface orientation, but a comprehensive model for the role of the surface orientation in the kinetic mechanism is lacking. The results of several experiments designed to develop a better understanding of which surface properties are most important in establishing the oxidation rate are reported. The results indicate that the Si surface atom density is important in the initial stages of oxidation and a revised explanation for the crossover effect is proposed.

20 DISTRIBUTION/AVAILABILITY OF ABSTRACT	21 ABSTRACT SECURITY CLASSIFICATION
☒ UNCLASSIFIED/UNLIMITED ☒ SAME AS RPT ☐ DTIC USERS	Unclassified
22a NAME OF RESPONSIBLE INDIVIDUAL Dr. David L. Nelson	22b TELEPHONE (Include Area Code) (202) 696-4410 22c OFFICE SYMBOL

DD FORM 1473, 84 MAR 83 APR edition may be used until exhausted
All other editions are obsolete

SECURITY CLASSIFICATION OF THIS PAGE

"The Effect of Surface Orientation on Silicon Oxidation Kinetics"

E.A. Lewis and E.A. Irene
Department of Chemistry
The University of North Carolina
Chapel Hill, North Carolina 27514

keywords: stress, Si orientation

ABSTRACT

It is well established that the rate of thermal oxidation of silicon depends on the surface orientation, but a comprehensive model for the role of the surface orientation in the kinetic mechanism is lacking. The results of several experiments designed to develop a better understanding of which surface properties are most important in establishing the oxidation rate are reported. The results indicate that the Si surface atom density is important in the initial stages of oxidation and a revised explanation for the crossover effect is proposed.

Introduction

The silicon surface orientation is an important parameter in the kinetic mechanism for the thermal oxidation of Si (1-11). Orientation dependent oxidation rates are observed at all temperatures in the range 600-1100°C (1-11). The order of the rates as a function of orientation is complex and depends on oxide thickness (7-9), oxidation temperature (3,7-9), and ambient pressure (1,6-8). In the initial stages of oxidation at 1 atm the rates are in the order (110) > (111) > (100), but within the first 25 nm of oxide formed, the order is reversed on the (110) and (111) orientations at temperatures in the range 750-1000°C (7,9-11). The thickness where the rate crossover occurs varies slightly with oxidation temperature, increasing with increasing temperature (7). Further complicating an understanding of the role of orientation in the kinetic mechanism is the crossover observed between the (111) and (100) orientations at partial pressures below 0.1 atm (6-8). None of the current models for Si oxidation can explain all aspects of the observed orientation dependent rate behavior described above. In order to model the effect of surface orientation on the oxidation kinetics it is necessary to identify which surface properties alter the rate and which steps in the kinetic mechanism are affected.

The oxidation process involves transport of the oxidant species to the Si-SiO_2 interface followed by a chemical reaction at the interface (12,13). The most widely accepted model for Si oxidation is the Deal-Grove model (14) which uses a linear-parabolic

expression (15) to fit the thickness, L, versus time, t, data as follows:

$$(L^2 - L_o^2)/ k_p + (L - L_o)/ k_l = t - t_o.$$

This model is derived from a steady state analysis of a diffusive transport flux in series with a first order interface reaction. The parabolic rate constant, k_p, is proportional to the effective diffusivity of oxidant through the SiO_2 film, and the equilibrium concentration of oxidant in the oxide, C^*. The linear rate constant, k_l, is proportional to the interface reaction rate constant, k_r, and C^*. L_o and t_o are offsets in thickness and time, respectively, and define an initial regime where the oxidation rate is greater than predicted by the model. Applying this model to experimental data it is found that both k_p and k_l are orientation dependent (2,4,5,9). Although the Deal-Grove model provides a basis for analyzing the kinetic data and allows for orientation dependent rates through k_r, it does not explicitly account for the observed orientation behavior.

Other studies have suggested possible sources for the orientation dependent rates including variations in the number of Si-Si bonds available for reaction (1,5), the orientation of bonds on the surfaces (1,16), and the density of surface steps (17,18). At temperatures below 1000°C the oxidation rate may be further influenced by intrinsic oxide stress (10,19). The presence of an intrinsic stress having a magnitude on the order of 10^9 dynes/cm^2 at oxidation temperatures below approximately 1000°C is well established (20-24).

Several modifications to the Deal-Grove model have introduced orientation dependent parameters such as stress (25-28) and the Si surface atom density (25) into the rate constants to explain the orientation dependence. However, it is not clear whether stress increases the oxidation rate by enhancing the interface reaction rate (25), or decreases the oxidation rate by reducing the diffusivity of oxidant through the oxide (26-28). The goal of this study was to determine the effect of stress and Si surface atom density on the oxidation rate at 1 atm. There is not sufficient data available on the variation of surface steps with orientation, or on the effect of bond orientation on the oxidation rate to determine their role in the orientation dependence.

The results of oxidation experiments at 700°C, 1000°C and 1100°C using five Si orientations are presented. The use of an extended range of orientations provided a broad basis for comparison of the oxidation rates with Si surface properties. It is difficult to extract accurate rate constants from the kinetic data, especially at low temperatures where the oxide thickness range covered in a typical oxidation experiment is small. Therefore, in this study the kinetic data was analyzed in terms of oxidation rate as a function of oxide thickness, i.e. the slope of the thickness versus time curve at a given film thickness. This enabled a model independent analysis of the oxidation process as a function of both oxide thickness and Si orientation. For oxidations at 700°C it was anticipated that the slow growth rate would limit the oxidation to a thickness regime where only the interface reaction kinetics were important in controlling the oxidation rate. At

this temperature the intrinsic oxide stress is high (23,24) and the effect of oxide stress on the interface reaction was expected to be maximized. In order to separate stress effects from other orientation dependent parameters, a second set of oxidation experiments using all five orientations was carried out at 1000°C. Stress relaxation is observed at temperatures above 970°C (20) and thus, at 1000°C the intrinsic stress is greatly reduced (21,23,24). However, experimental stress measurements show a low residual intrinsic stress is present even in oxides grown at 1000°C (24). To determine if the crossover was affected by stress, oxidations were done at 1100°C which is well above the temperature required for viscous relaxation. The results lend new insight into the crossover effect and the importance of surface atom density in establishing the oxidation rate.

Experimental

Commercially available single crystal Si wafers with a resistivity of 2-10 ohm-cm and having the orientations (110), (111), (311), (511) and (100) were oxidized at 1 atm at 700°C, 1000°C and 1100°C in pure dry oxygen. The (311) and (511) orientations were N-type wafers while the other orientations were P-type but in this resistivity range the oxidation rate is independent of dopant type (5). All oxide thickness measurements were made with a research quality ellipsometer using 632.8 nm light. The samples were cleaned immediately before oxidation using a modified RCA (29) procedure followed by a 10 sec HF dip and DI water rinse. It has been

established that the initial oxidation rates vary with the wafer cleaning procedure (30,31). To insure the validity of the results presented here, all samples were cleaned identically and the conclusions are based on relative rather than absolute oxidation rates.

The 700°C oxidation kinetics were measured in-situ with an oxidation furnace mounted at the focus of the ellipsometer (32). Optical constants were obtained from previously published data (22,32). The samples were heated to the oxidation temperature in N_2 for 15 min before changing to an O_2 ambient. The O_2 and N_2 were of high purity having an H_2O content of less than 1 ppm measured at the outlet of the oxidation furnace. Kinetic data was collected over 46-52 hour time intervals. The oxide thickness obtained in this time was less than 30 nm on all samples. The oxidation rate was slow enough that manual null ellipsometric measurements could be made during the oxidation to obtain accurate thickness values (approximately 1% error).

The kinetic data at 1000°C was not collected in-situ but instead from a series of oxidations using a conventional oxidation furnace having a double-walled fused silica furnace tube. A preburner-condenser apparatus (5) was placed in series with the oxidation furnace to remove H_2O and hydrocarbons from the oxidizing ambient. The measured H_2O content was less than 3 ppm at the furnace outlet. Kinetic data was collected from eight oxidations ranging in time from 0.5 to 16 hours and covering the thickness range 25-300 nm. Samples of

the five orientations were oxidized simultaneously, removed from the furnace and measured ellipsometrically. For each oxidation run the samples were flushed with dry N_2 in the end cap then brought to oxidation temperature at the center of the furnace hot zone in an N_2 ambient. The samples also received a 15 minute post oxidation anneal in N_2. The thickness data is the average of four ellipsometric measurements (2 per wafer with 2 wafers of each orientation). This type of experiment confirms the order of the relative rates since all orientations are oxidized simultaneously. In the in-situ experiments each orientation is oxidized in separate runs, and thus, the relative rates may vary slightly since it is difficult to maintain the exact oxidation conditions from run to run.

At 1100°C extensive data sets were collected on the (111) and (110) orientations and two oxidations included all five orientations. The same apparatus described for the 1000°C oxidations was used at 1100°C, but the pre-oxidation heating and post-oxidation annealing were done in an Ar ambient to prevent the formation of an interfering Si_3N_4 film (33). The H_2O content in the oxidizing ambient was less than 4 ppm measured at the furnace outlet.

Results

As explained above, the data was analyzed in terms of oxidation rate as a function of thickness and orientation. The results of the 700°C oxidation experiments plotted as oxide thickness versus time are

shown in Figure 1. There is a distinct orientation dependent oxidation rate on all five orientations. The initial oxidation rate decreased rapidly with thickness on all orientations and could be fit to two decaying exponential functions, with one extending to about 3 nm and the second extending from 3 to 10 nm. Similar rate behavior in the initial stages of oxidation was reported by Massoud et. al. for oxidations in the temperature range 800-1000°C (7,8). Beyond 10 nm the oxidation rate as a function of thickness was determined analytically from a second degree polynomial fit to the data. This corresponds to a linear-parabolic form for the equation. Oxidation rates, i.e. the slope of the fitted functions, at 700°C for several oxide thicknesses on the five orientations are presented in Table 1. The oxidation rates are in the order:

$$(110) > (111) > (311) > (511) > (100)$$

up to a thickness of 25 nm. However, the difference in rates on the (110) and (111) surfaces decreases with thickness and a crossover in rate to (111) > (110) occurs near 25 nm. The thickness where the crossover in rate is observed is greater than expected based on the results of earlier studies over the temperature range 750-1000°C (7,11). The discrepancy may reflect subtle differences in the exact pre-oxidation cleaning procedure (30,31) or oxidation conditions. A second crossover thickness has been defined at the actual thickness where a crossover is observed in plots of thickness versus time (7). This crossover point is not observed in the 700°C data presented here, (Figure 1), because the oxidation rate was so

slow that the thickness where a crossover in L-t occurs was not reached within the 48 hour oxidation. The other three orientations maintain the same order throughout the thickness range covered in this time interval.

The 1000°C data showed the same orientation dependence as the 700°C oxidations. The (110) and (111) surfaces had the highest oxidation rates with the initial order (110) > (111). Because of the faster oxidation rate at 1000°C, the thickness where a crossover in both rate versus thickness (L=10 nm) and thickness versus time (L=40 nm) occurs was reached within the first hour of oxidation. These crossover thicknesses are consistent with previously reported data (7). The rates on the (311), (511) and (100) surfaces were in the same order as at 700°C with the thickness range extended to 250 nm at 1000°C. Thus, the order of the rates on these three orientations was not changed by decreasing the intrinsic oxide stress. The data collected in the region before the rate crossover is not sufficient to determine the rates from functional fits, but second degree polynomial fits were used to determine the rates at thicknesses beyond 25 nm. The rates at 1000°C relative to the (100) orientation in several thickness ranges are included in Table 5 which is discussed later. The order of the rates beyond the crossover, determined in this study for dry O_2 oxidations, is the same as the order reported by Pliskin (2) for 1 atm steam oxidations at 971°C using the (111), (110), (311) and (100) orientations. However, both 1 atm studies exhibit an orientation dependence which differs from the high pressure results obtained by Ligenza (1).

At 1100°C the crossover behavior on the (110) and (111) surfaces was different than at lower temperatures (700-1000°C). A partial data set from the oxidations at 1100°C on the (110) and (111) surfaces is shown in Table 2. The reported thicknesses are the average of four ellipsometric measurements on two samples of each orientation. The thickness for the one hour oxidation was sufficient to calculate an index of refraction for these films of 1.459. It is seen from Table 2 that for oxidation times extending to 24 hours the oxide thickness on the (110) surface is always greater than on the (111) surface. The maximum variation in the measured thicknesses was ±1 nm and thus, the observed order is not due to differences in thickness across the wafer or differences in the position of the wafers in the furnace. A crossover is not observed in a plot of thickness versus time for thicknesses extending to 700 nm. In contrast, for oxidations in the temperature range 800-1000°C the crossover in thickness versus time plots to (111) > (110) occurs within the thickness range 15-40 nm (8). The oxidation rates, determined from second degree polynomial fits to the entire data set, converge with increasing oxide thickness but do not exhibit a crossover. Oxidations on all five orientations showed that the inial order of the rates observed at 700°C and 1000°C is maintained to a much larger thickness (several hundred nm) at 1100°C.

In summary, the initial oxidation rates follow the order (110) > (111) > (311) > (511) > (100). This order changes within the first 30 nm of oxide formed for 700°C < T_{ox} < 1000°C to (111) > (110) with the other orientations retaining the same order. At 1100°C the

order for all thicknesses 0-700 nm is identical to that observed at lower temperatures in the precrossover region.

Discussion

In order to understand the role of the Si surface orientation in the oxidation mechanism, it is important to establish whether the rate is controlled by diffusional transport or by the interface reaction. The rate limiting process in these experiments was determined by comparing the flux of O_2 that reacted at the interface, F_R, with the calculated diffusive flux of O_2, F_D, at the oxidation temperature (34). The reaction flux is observed experimentally and is calculated from the oxidation rate as $F_R = \Omega \dot{L}$ where Ω is the number of O_2 molecules incorporated into a unit volume of SiO_2 and $\dot{L}$ is the oxidation rate. The diffusive flux of O_2 in SiO_2 has not been measured directly. However, F_D is related to the parabolic rate constant defined in the Deal-Grove model (14). Thus, an approximate value was calculated using previously published k_p values at 1000°C and extrapolated values at 700°C (9). The k_p value used for 1100°C was determined from the data collected in this experiment. The calculated ratio F_D / F_R in several thickness regimes is shown in Table 3 for the (100) orientation at 700°C and 1000°C and for the (111) orientation at 1100°C. Similar results were obtained on the (110) orientation. In all cases, the ratio F_D / F_R is greater than one which means that the oxidation is not diffusion limited although a diffusion limited regime is approached at 1100°C for thicknesses above 300 nm. The lack of a direct measurement of the diffusivity and the validity of applying a

Fickian diffusive mechanism to the thin films obtained at 700°C are sources of error in the calculation. However, based on the available data used for this calculation, it is concluded that the oxidation rate is controlled by the interface reaction rate in the thickness regimes covered by these experiments.

To determine whether the Si surface atom density, N_{Si}, was an important parameter controlling the oxidation rates, the order of the rates was compared with N_{Si} as a function of orientation. If the interface reaction rate is dependent on the Si surface atom density, N_{Si}, (25) then the experimental rates on the five orientations should parallel the order of N_{Si} with orientation. Calculated values for N_{Si} as a function of orientation were published by Ligenza (1) and are shown in the second column of Table 4 along with the value for N_{Si} on the (511) plane which was calculated using the same method. A small correction to the previously published N_{Si} value for the (311) plane (1) has been made, but does not change the order of N_{Si} with orientation. The method used to calculate these numbers is described in Appendix 1. It is seen from column 2 of Table 4 that the order of the N_{Si} values calculated using this method is:

$$(511) > (311) > (110) > (111) > (100)$$

which differs from the experimental order of the oxidation rates (see Table 1). The apparent discrepancy between the calculated and experimental results can be explained using the results of LEED and RHEED studies on the (311) and (511) planes (35,36). These planes are

vicinal surfaces to the (100) plane and are not structurally stable. The (311) and (511) surfaces reconstruct to form a stepped surface having (100) oriented terraces and (111) oriented step edges. The areal ratio of (111) to (100) oriented regions on the reconstructed surface is determined by the initial interplanar angle between the vicinal surface and the (100) plane. Since values for N_{Si} on the reconstructed (311) and (511) surfaces have not been reported, a calculation was made based on the available information (see Appendix 2). The results are shown in Column 3 of Table 4. These calculated values represent effective surface atom densities since there are actually regions of two different orientations on the same surface. Using the corrected values for N_{Si} on the reconstructed (311) and (511) surfaces, qualitative agreement is obtained between the order of the initial rates and the Si surface atom density. The initial rates on the five orientations increase in the same order as the actual Si surface atom density.

Table 5 presents a quantitative analysis of the relationship between the surface atom density and the relative rates in several thickness ranges at 700°C and 1000°C. All ratios are with respect to the (100) surface. It is clear from Table 5 that although the initial oxidation rates at 700°C scale qualitatively with N_{Si}, they do not scale quantitatively. The rate ratios are substantially greater than predicted based on N_{Si} which indicates that surface atom density is not the only parameter affecting the initial oxidation rate. The lack of a quantitative scaling may reflect differences in reaction rates caused by the orientation of bonds on the surface, stress effects or

other properties related to the reactivity of the surface atoms. The effect of stress, if significant, should be greatest at the lower oxidation temperatures where the stress is largest. However, based on the results at 700°C and 1000°C, it is also clear that stress does not affect the order of the rates before the crossover. The (110), (311) and (100) orientations have similarly high intrinsic stress values while the (111) orientation has the lowest measured stress (11,24). The order of the initial rates does not correlate with this trend in stress and is not changed when stress levels are reduced at higher temperatures. Thus, while stress may alter the absolute rates, the overall order of the initial rates remains unaffected. It is concluded that the surface atom density is the most important parameter establishing the order of the initial rates.

Extending the analysis to thicker films using the 1000°C data, it is seen from Table 5 that beyond 50 nm there is relatively good agreement between the rate ratios and the ratio of N_{Si} on the (110), (311), (511) and (100) surfaces. The rate ratio on the (111) surface is higher than predicted. Thus, except for the (111) orientation, it appears that even beyond the crossover thickness the Si surface atom density is important in controlling the oxidation rates for thicknesses up to 200 nm. The anomolously high rate on the (111) is related to the crossover which is discussed below.

The crossover reflects a thickness dependent parameter which either increases the rate on the (111) surface relative to the (110), or decreases the rate on the (110) surface relative to the (111). The

mechanism causing the crossover is not well understood. To date the only model for this behavior involved a stress enhanced interface reaction on the (111) orientation (10), but recent stress measurements showed that the (110) orientation has a higher intrinsic stress than the (111) orientation (11,24). Thus, the crossover cannot be caused by a stress enhanced interface reaction on the (111) surface. However, the results from the 1100°C oxidations reported here indicate that the crossover may be related to the intrinsic stress. At 1100°C, where intrinsic stress is reduced to its lowest value (11,24,25), a crossover is not observed. Since the crossover observed at lower temperatures is not due to a stress enhanced reaction on the (111), an alternate explanation based on a stress related decrease in rate on the (110) surface is proposed.

The decrease in rate on the (110) surface is attributed to a decrease in the diffusion rate through the SiO_2 film since a compressive oxide stress is expected to lower the diffusion rate (27,37). It was determined above that the oxidation rate is controlled by the interface reaction in the thickness range considered here. A simple first order rate law for this process is given by $F_R = k_r C_i$ where k_r is the interface reaction rate constant and C_i is the concentration of oxidant at the interface (14). Although it was concluded that the initial order of the rates is determined by the surface atom density (through k_r), C_i may be affected by stress as the oxide thickness increases. If C_i is reduced due to a decreased rate of diffusion, then a corresponding decrease in the interface reaction rate is anticipated. This is equivalent to reducing the partial pressure of O_2 in the ambient. Since the (110) has the highest

intrinsic stress (10,24), the diffusion rate and thus C_i would be reduced the most on this orientation. The diffusion process, and therefore C_i, on the (111) orientation would be least affected by stress. If C_i on the (111) orientation becomes higher than on the (110) orientation, then this difference may compensate for the difference in N_{si} and result in the crossover in rate to (111) > (110). This model assumes that the stress level is sufficient to alter the diffusivity. A higher diffusivity on the (111) orientation relative to the (110) and (100) orientations, as required by this explanation, is supported by k_p values derived from applying the Deal-Grove model to oxidation data in the temperature range 800-1000°C (9). In the Deal-Grove model k_p values are directly proportional to the diffusivity of O_2 through the oxide. k_p values determined at temperatures below 950°C (9) are the highest on the (111) orientation and thus indicate that at lower temperatures the diffusivity of O_2 through the oxide on the (111) is greater than on the (110) orientation. Although this model for the crossover will require further experimental justification, it is consistent with the currently available data.

SUMMARY

It is concluded that the Si surface atom density is the most important surface property establishing the order of the initial oxidation rates. A quantitative scaling of oxidation rate with surface atom density is not observed in the thickness range 0-30 nm. Thus, other orientation dependent parameters alter the absolute rates but do

not change the order of the rates in the thickness regime before the crossover. For film thicknesses beyond the crossover at 1000°C the rates scaled in approximately the same ratios as the surface atom density except on the (111) orientation. An explanation for the crossover in rate between the (110) and (111) orientations is still not clear. However, at 1100°C a crossover is not observed and the initial order of the rates, (110) > (111) is maintained at thicknesses up to 700 nm. A model for the crossover based on a stress related decrease in the diffusivity on the (110) plane at lower temperatures was proposed.

Appendix 1

Calculating the Si surface atom density using the method described by Ligenza (1) involves determining the number of Si atoms located on a specific plane in the Si unit cell, and dividing by the area of that plane. The area of the (100) and (110) planes is easily determined. The calculation for the area of the (311) plane is described below since the value determined here differs from Ligenza's value (1). The area of the (511) and (111) planes directly parallels the calculation on the (311) plane. Referring to Figure 2 where a is the lattice parameter of the Si unit cell, the area of the (311) plane is calculated as follows:

$AB = BC = \sqrt{(a^2 + (a/3)^2)} = \sqrt{(10)} * a/3$

$AC = \sqrt{(2)} * a$

$BD = \sqrt{((AB)^2 - (AD)^2)} = \sqrt{(10/9*a - 1/2*a)}$

So,

$BD = 1/3 * \sqrt{(11/2)} * a$

$Area = 0.5 * (AC) * (BD) = 1/6 * \sqrt{(11)} * a^2$

The areas of all five orientations are given in Table 6.

The next step is to determine the fractional number of Si atoms located on each plane within one unit cell. The calculated value includes only the circular projection of the Si atom (assumed spherical) on the plane area. For the (100), (110) and (111) planes the calculation is direct, but for the (311) and (511) orientations there is some ambiguity in determining the number of Si atoms on the plane. On both planes the atom located at (0,¾,¾), D in Figure 2,

contributes 0.5 to the total number of Si atoms. For the (311) plane, the atoms located at (0,1,0) and (0,0,1), A and C in Figure 2, contribute the fraction 47.9/360 to the number of atoms on the plane since the angles ACB and CAB are 47.9°. On the (511) plane these atoms contribute the fraction 46.1/360. The ambiguity in counting the number of Si atoms on these surfaces arises from the treatment of the atom located at (¼,¼,¼). This atom does not lie directly in the plane for these two orientations but is very close. The perpendicular distance from the atom at (¼,¼,¼) to the (311) plane is 0.04 nm and to the (511) plane is 0.08 nm. In calculating the surface atom densities on these two plane it was assumed that this atom contributed 1 to the total number of Si atoms even though it is not directly on the plane. Thus, the number of atoms on the (311) plane is 1.77 and on the (511) plane is 1.76. As discussed previously in the paper, the results of LEED and RHEED studies on these surfaces (35,36) show that there really is no ambiguity concerning the contribution of this atom. The structure of the as cleaved surfaces on the (311) and (511) planes are not stable and reconstruct to form a surface consisting of (100) and (111) regions. A summary of the calculated surface atom densities not considering any changes to the surface structure upon cleaving is presented in Table 6. The corrected values for N_{si} on these two planes taking into account the reconstructed surface are calculated in Appendix 2.

Appendix 2

In order to calculate the effective surface atom density on the (311) and (511) planes it is necessary to calculate the areal ratio of (100) to (111) oriented regions on the reconstructed surfaces. This calculation is based on descriptions of the (100) vicinal surfaces provided by LEED and RHEED studies (35,36). Figures 3 and 4 depict the essential features of the calculation for the (311) plane. Consider the area ABCD in Figure 3 which has the (311) orientation and extends over two unit volumes, w^3, of the Si crystal where w is an integral number of unit cell lengths. The edges of the unit volume are oriented along <100> directions. According to the model for the vicinal (100) surfaces (35), the original (311) plane reconstructs to form a more stable surface consisting of (100) terraces and (111) steps. This surface structure is represented by the dashed lines in Figure 3 where $a_{\langle 100 \rangle}$ represents the area of each terrace and $a_{\langle 111 \rangle}$ is the area of a step. The ratio of the area of (100) to (111) oriented regions in ABCD is given by

$$A_{\langle 100 \rangle} / A_{\langle 111 \rangle} = \Sigma\, a_{\langle 100 \rangle} / \Sigma\, a_{\langle 111 \rangle} \qquad (1).$$

The areas $a_{\langle 100 \rangle}$ and $a_{\langle 111 \rangle}$ are parallelograms having the same height, h, but different widths $w_{\langle 100 \rangle}$ and $w_{\langle 111 \rangle}$. The area of each terrace is then

$$a_{\langle 100 \rangle} = w_{\langle 100 \rangle} \times h \qquad (2a)$$

and the area of a step is

$$a_{\langle 111 \rangle} = w_{\langle 111 \rangle} \times h \qquad (2b).$$

Thus, the areal ratio of (100) to (111) surfaces is

$A_{\langle 100 \rangle} / A_{\langle 111 \rangle} = \Sigma a_{\langle 100 \rangle} / \Sigma a_{\langle 111 \rangle} = \Sigma w_{100} / \Sigma w_{111}$ (3)

and the problem reduces to the 2 dimensional situation depicted in Figure 4 which shows the region OCD from Figure 3. The angle θ is the angle between the $\langle 1\bar{1}0 \rangle$ direction (i.e. the intercept of the (111) plane with the (001) plane) and $\langle 0\bar{1}0 \rangle$ direction which is 45°. It is necessary to calculate the ratio $\Sigma w_{\langle 100 \rangle} / \Sigma w_{\langle 111 \rangle}$ under the restrictions :

$\Sigma h_{step} = w/3$ (4)

and

$\Sigma w_{\langle 100 \rangle} + \Sigma w'_{\langle 111 \rangle} = w$ (5)

where h_{step} is the step height, w/3 is the distance OC where the (311) plane intersects an edge of the unit volume and $w'_{\langle 111 \rangle}$ is the projection of the (111) step edge along the <100> direction. The number of steps on this surface, N_s, is given by

$N_s = (w/3) / h_{step}$ (6).

Other useful expressions from figure 4 are :

$w'_{\langle 111 \rangle} = h_{step} / \tan(45^\circ) = h_{step}$ (7)

and

$w_{\langle 111 \rangle} = h_{step} / \sin(45^\circ) = \sqrt{2} * h_{step}$ (8).

Using the above expressions, $\Sigma w_{\langle 100 \rangle}$ and $\Sigma w_{\langle 111 \rangle}$ can be derived as follows:

Rearranging equation (5),

$\Sigma w_{\langle 100 \rangle} = w - \Sigma w'_{\langle 111 \rangle}$ (9).

Using equations (6) and (7),

$\Sigma w'_{\langle 111 \rangle} = N_s \times w'_{\langle 111 \rangle} = w/3$ so,

$\Sigma w_{\langle 100 \rangle} = w - w/3 = 2*w/3$ (10).

Using equations (6) and (8),

$$\Sigma w_{(111)} = N_s * w_{(111)} = \sqrt{2}*w/3 \qquad (11).$$

Thus, the areal ratio of (100) to (111) oriented regions on the reconstructed (311) surface is

$\Sigma w_{(100)} / \Sigma w_{(111)} = (2*w/3)/ (\sqrt{2}*w/3) = 1.414.$

For the (511) plane the calculation is identical to that on the (311) plane except the number of steps, N_s is $(w/5)/h_{step}$ instead of $(w/3)/h_{step}$. The areal ratio (100):(111) on the reconstructed (511) surface is 2.83. An effective Si surface atom density, N_{Si}, can be calculated for these surfaces using the areal ratios and the N_{Si} on the (100) and (111) planes:

$N_{Si} = A_{(100)}/A_{tot} * N_{Si(100)} + A_{(111)}/A_{tot} * N_{Si(111)}$

where $A_{tot} = A_{(100)} + A_{(111)}$.

For the (311) orientation this is calculated to be 7.21×10^{14} atoms/cm^2 and for the (511) orientation 7.05×10^{14} atoms/cm^2.

Acknowledgment

This work was supported in part by the Office of Naval Research (ONR).

References

1) J.R. Ligenza, J. Phys. Chem., 65, 2011 (1961).
2) W.A. Pliskin, IBM J. Res. Dev., 10, 198 (1966).
3) B.E. Deal, J. Electrochem. Soc., 110, 527 (1963); 110 , 1292 (1963).
4) Y.J. van der Meulen, J. Electrochem. Soc., 119, 530 (1972).
5) E.A. Irene, J. Electrochem. Soc., 121, 1613 (1974).
6) S.I. Raider and L.E. Forget, J. Electrochem. Soc., 127, 1783 (1980).
7) H.Z. Massoud, PhD. Thesis, Stanford University (1983).
8) H.Z. Massoud, J.D. Plummer and E.A. Irene, J. Electrochem. Soc., 132, 2685 (1985).
9) H.Z. Massoud, J.D. Plummer, and E.A. Irene, J. Electrochem. Soc., 132, 1745 (1985).
10) E.A. Irene, H.Z. Massoud and E.Tierney, J. Electrochem Soc., 133, 1253 (1986).
11) E.A. Lewis, E. Kobeda and E.A. Irene, "Proceedings of the Fifth International Symposium on Silicon Materials Science and Processing", The Electrochemical Soc., Ed. by H.R. Huff, Boston, Mass. May (1986).
12) W.A. Pliskin and G.P. Gnall, J. Electrochem. Soc., 111, 872 (1964).
13) F. Rochet, B. Agius and S. Rigo, J. Electrochem. Soc., 131, 914 (1984).
14) B.E. Deal and A.S. Grove, J. Appl. Phys., 36, 3770 (1965).
15) U.R. Evans, The Corrosion and Oxidation of Metals, (Edward Arnold and Company, London, 1960), pp 819-859.
16) R. Ghez and Y.J. van der Meulen, J. Electrochem. Soc., 119, 1100 (1972).
17) N. Mott, Proc. R. Soc. London, 376, 207 (1981).
18) P.O. Hahn and M. Henzler, J. Vac. Sci. and Technol. A, 2, 574 (1984).
19) W.A. Tiller, J. Electrochem. Soc., 127, 619 (1980).
20) E.P. EerNisse, Appl. Phys. Lett., 30, 290 (1977).
21) E.P. EerNisse, Appl. Phys. Lett., 35, 8 (1979).
22) E.A. Irene, D.W. Dong and R.J. Zeto, J. Electrochem. Soc., 127, 396 (1980).
23) E. Kobeda and E.A. Irene, J. Vac. Sci. and Technol. B, 4, 720 (1986).
24) E. Kobeda and E.A. Irene, J. Vac. Sci. and Technol. B, submitted for publication, 1986.
25) E.A. Irene, J. Appl. Phys., 54, 5416 (1983).
26) R.H. Doremus, Thin Solid Films, 122, 191 (1984).
27) A. Fargeix and G. Ghibado, J. Appl. Phys., 54, 153 (1983).
28) A. Fargiex and G. Ghibado, J. Appl. Phys., 56, 589 (1984).

29) W. Kern and D.A. Puotinen, RCA Review, 31, 187 (1970).
30) F.N. Schwettman, K.L. Chiang, and W.A. Brown, Abs. No. 276, Extended Abstracts, Vol 78-1, The Electrochemical Soc., Seattle, WA. May (1978).
31) G. Gould and E.A. Irene, J. Electrochem. Soc., submitted for publication, (1986).
32) Y.J. van der Meulen and N.C. Hien, J. Opt. Soc. America, 64, 804 (1974).
33) S.I. Raider, R.A. Gdula and J.R. Petrak, Appl. Phys. Lett. 27, 150 (1975).
34) E.A. Irene, Phil. Mag., submitted for publication (1986).
35) K. Ueda and M. Inoue, Surface Sci., 61, L578 (1985).
36) B.Z. Olshanetsky and A.A. Shklyaev, Surf. Sci., 82, 445 (1979).
37) G. Camera Roda, F. Santarelli, and G.C. Sarti, J. Electrochem. Soc., 132, 1909 (1985).

LIST OF TABLES

Table 1. OXIDATION RATES AT 700°C in (nm/min) AS A FUNCTION OF OXIDE THICKNESS FOR FIVE Si ORIENTATIONS.

SILICON ORIENTATION	OXIDATION RATE AT THE FOLLOWING THICKNESSES: 5 nm	10 nm	20 nm	30 nm
(110)	0.196	0.129	0.094	0.074
(111)	0.130	0.102	0.088	0.077
(311)	0.125	0.089	0.066	
(511)	0.103	0.074	0.058	
(100)	0.075	0.057	0.044	

TABLE 2. PARTIAL THICKNESS VERSUS TIME DATA SET FOR OXIDATION AT 1100°C.

OXIDATION TIME (HRS)	OXIDE THICKNESS (nm) (110)	(111)
1	133.5	124.8
6	343.3	333.0
16	581.7	565.0
24	720.6	706.3

Table 3. RATIO OF DIFFUSIVE FLUX TO EXPERIMENTAL FLUX IN SEVERAL THICKNESS REGIMES.

	X_{ox} (nm)	F_D / F_{exp}
(100) Si at 700°C	5	7.44
	10	4.90
	20	3.18
(100) Si at 1000°C	30	9.29
	50	6.81
	200	4.70
(111) Si at 1100°C	100	1.49
	300	1.16
	500	1.10
	700	1.07

TABLE 4. Si SURFACE ATOM DENSITY VERSUS ORIENTATION

SILICON ORIENTATION	N_{si} BY METHOD OF LIGENZA (1) (APPENDIX 1) Si atoms/cm² (10^{14})	CORRECTED N_{si} BASED ON LEED MODEL (35,36) (APPENDIX 2) Si atoms/cm² (10^{14})
(110)	9.59	
(111)	7.83	
(311)	10.86	7.21
(511)	11.48	7.05
(100)	6.78	

TABLE 5. A QUANTITATIVE COMPARISON OF OXIDATION RATE AT 700°C AND 1000°C WITH Si SURFACE ATOM DENSITY

ORIENTATION	RATE RATIOS RELATIVE TO THE (100) AT THE FOLLOWING OXIDE THICKNESSES:				N_{si} RELATIVE TO THE (100)
	700°C		1000°C		
	10 nm	20 nm	50 nm	300 nm	
(110)	2.26	2.14	1.51	1.22	1.41
(111)	1.79	2.00	1.80	1.45	1.15
(311)	1.56	1.50	1.20	1.14	1.06
(511)	1.30	1.31	1.08	1.07	1.04
(100)	1.00	1.00	1.00	1.00	1.00

Table 6. CALCULATED SILICON SURFACE ATOM DENSITY

ORIENTATION	PLANE AREA in UNIT CELL	ATOMS ON PLANE IN UNIT CELL	Si atoms/cm^2 (10^{14})
(110)	$\sqrt{2}a^2$	4.0	9.59
(111)	$1/2\sqrt{3}a^2$	2.0	7.83
(311)	$1/6\sqrt{11}a^2$	1.77	10.86
(511)	$3/10\sqrt{3}a^2$	1.76	11.48
(100)	a^2	2.0	6.78

$a = 5.431 \times 10^{-8}$ cm

LIST OF FIGURES

Figure 1

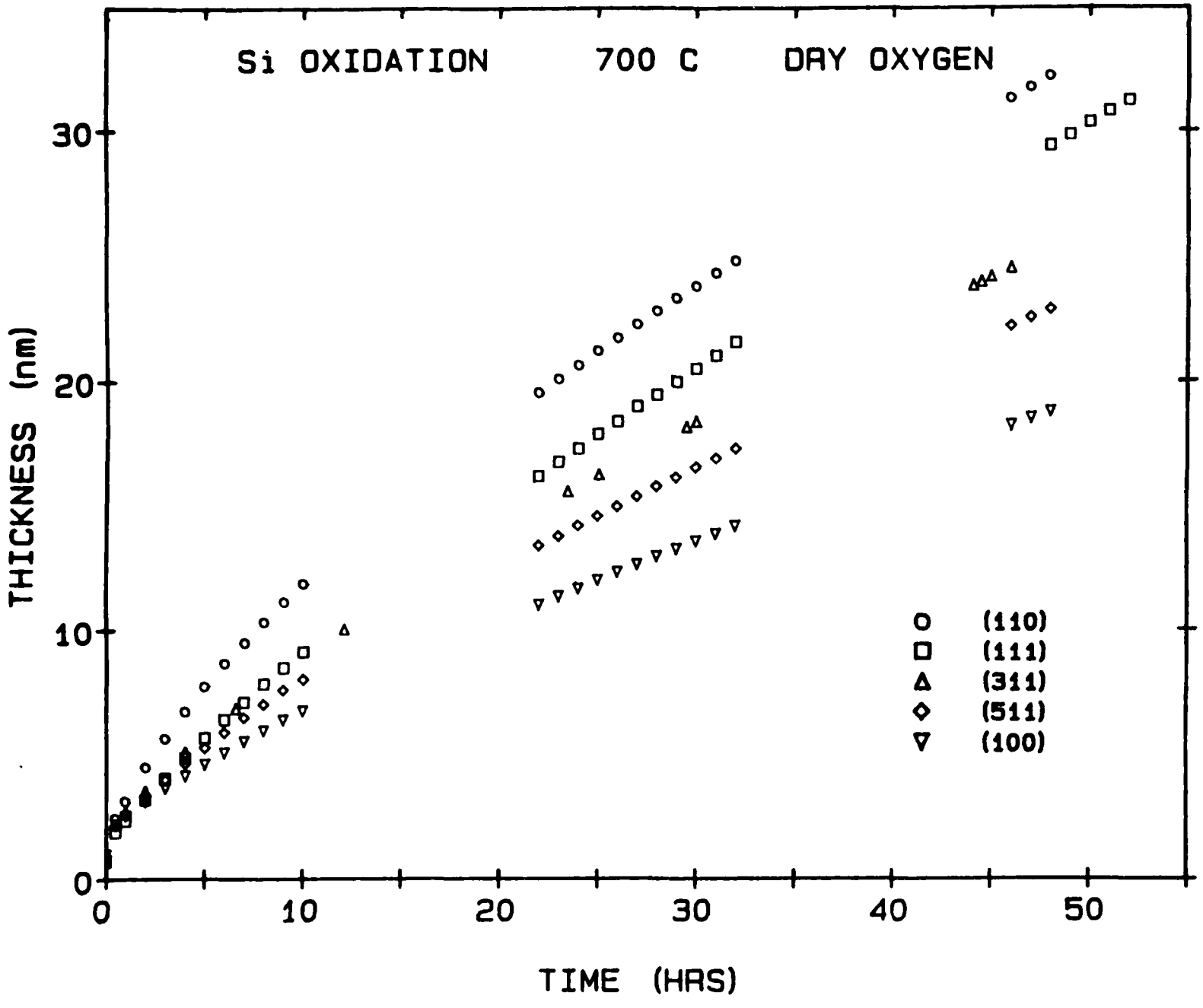
Si OXIDATION 700 C DRY OXYGEN
THICKNESS (nm)
TIME (HRS)
0
10
20
30
40
50
(110)
(111)
(311)
(511)
(100)

Figura 2

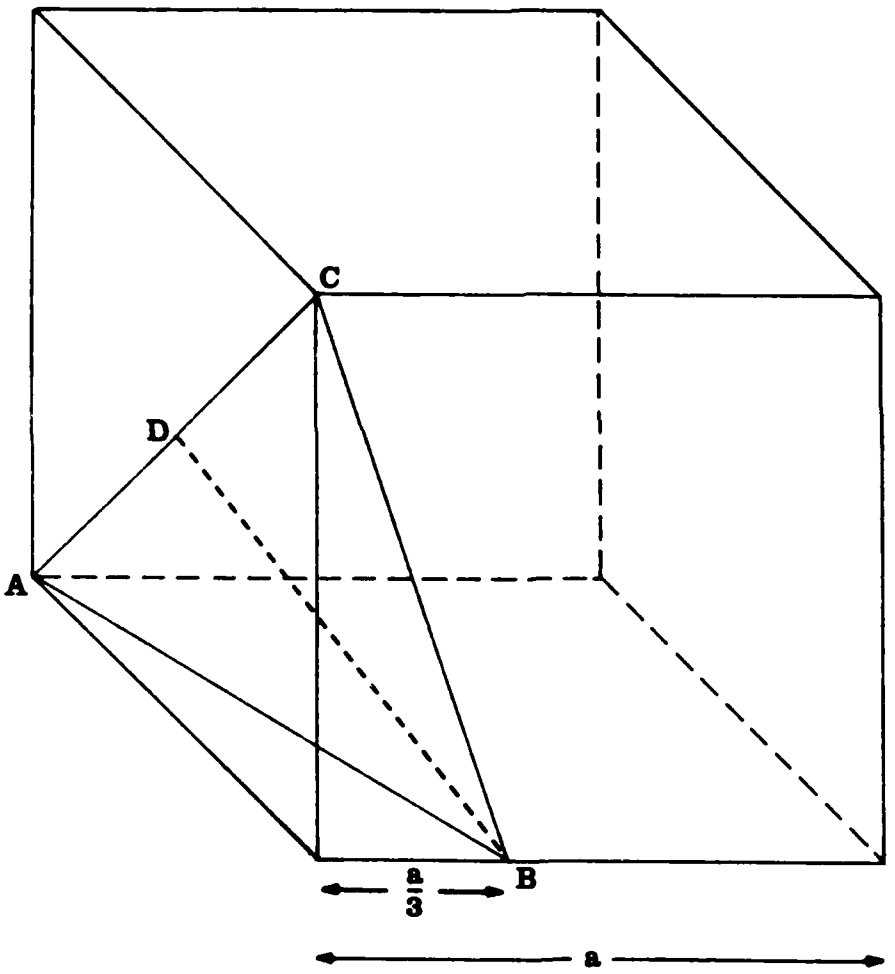

Figure 3

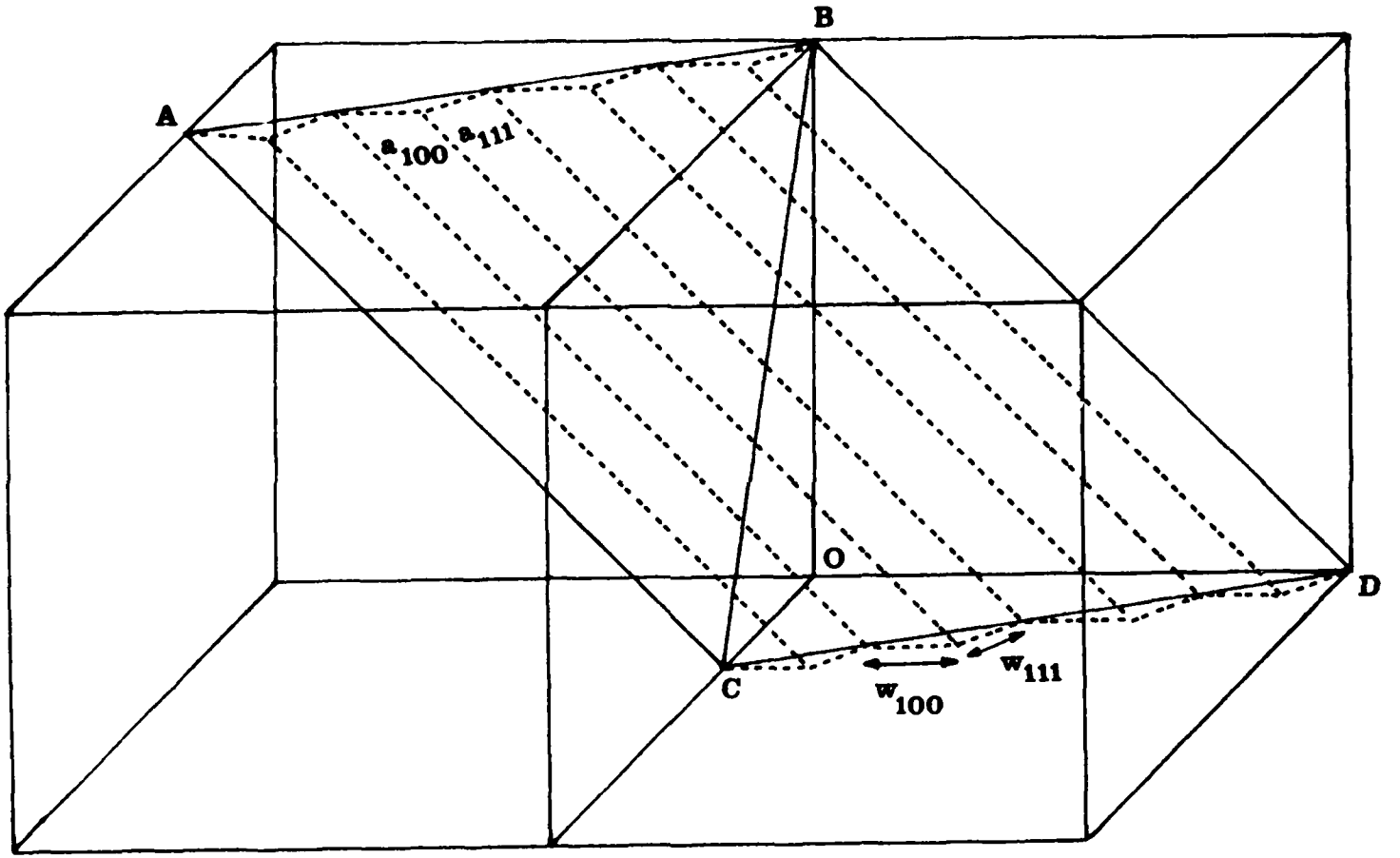

Figure 4

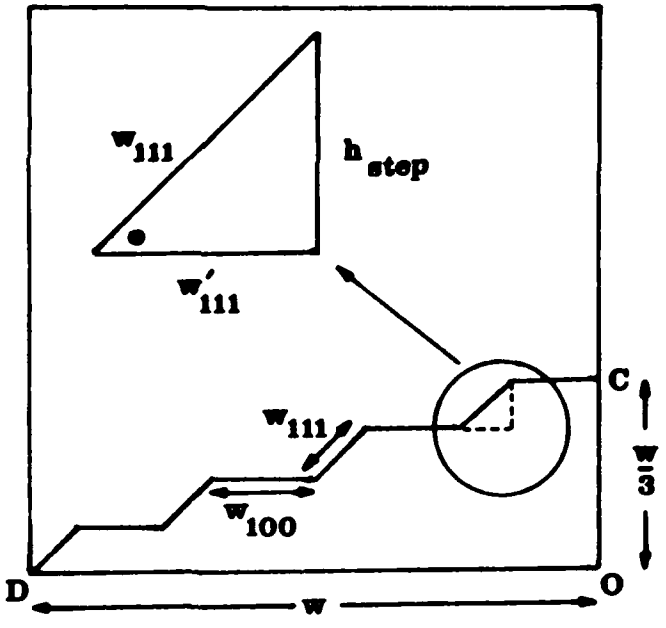

END

12-86

DTIC